ADVANCED OPTICAL MATERIALS
www.advopticalmat.de

Bottom-Up Tunable Broadband Semi-Reflective Chiral Mirrors

*Wenbing Wu, Yann Battie, Cyriaque Genet, Thomas W. Ebbesen, Gero Decher, and Matthias Pauly**

Conventional mirrors flip the handedness of circularly polarized light upon reflection. However, there is an increasing demand for the design and fabrication of handedness-preserving mirrors as well as chiral reflective metasurfaces with tunable spin states of reflected photons that work in a broad wavelength range in the UV and visible domain. Most chiral mirrors fabricated up to now are prepared by top-down techniques, such as e-beam lithography, which are very costly and difficult to scale up to macroscopic devices. Here, an efficient bottom-up strategy is introduced for fabricating chiral mirrors by using Layer-by-Layer assembly of oriented silver nanowire layers prepared by grazing incidence spraying on a semi-reflective silver layer. The resulting chiral metasurfaces display structure-dependent differential reflectance for circularly polarized light in a broad wavelength range in the UV, visible, and near infrared domains, reaching an extremely high figure of merit. Their differential reflectance reaches up to 95% of the maximum polarization efficiency, with the handedness of the reflected light being partially preserved. These large-area chiral mirrors with tunable chiral reflectance open perspectives in various fields, such as in optics, sensing, and chiral light-matter interactions.

1. Introduction

Conventional mirrors, such as metallic films or interference-based dielectric multilayer Bragg reflectors, flip the helicity of a photon upon reflection at normal incidence, which leads to a reversal in handedness of the reflected circularly polarized light (**Figure 1**a): left-handed circularly polarized (LCP) light is reflected as right-handed circularly polarized (RCP) light, and vice versa. However, there is an increasing demand for the design and fabrication of handedness-preserving mirrors[1] (Figure 1b) as well as chiral reflective metasurfaces with tunable spin states of reflected photons for potential applications in photon manipulation,[2] chiral cavities,[1b,3] sensing,[4] chiral quantum optics,[5] and chiral light-matter interactions.[6]

The present strategies for fabricating chiral mirrors mainly aim at creating 2D chiral patterns on a metallic surface[7] or on photonic crystal mirrors,[8] or exploit extrinsic chirality with non-chiral 2D patterns illuminated at oblique incidence.[9] It has also been predicted that twisted layers of oriented gold nanorods[10] and arrays of helices[11] provide highly chiral reflection. More importantly, most up-to-date reports of chiral mirrors either exhibit circular dichroic reflection in GHz[1a,2,12] to THz[13] range or have a very narrow chiral reflection peak. Some structures have chiral reflection in the near IR range,[8b,9–10] but this requires fabricating complex patterns at subwavelength scale, which imposes using top-down techniques, such as e-beam lithography. These techniques turn out to be very costly and difficult to scale up to macroscopic devices.

Designing chiral metasurfaces working at optical frequencies requires controlling the size, position, and direction of the individual building blocks at a nm scale, which is challenging for

W. Wu, G. Decher, M. Pauly
Université de Strasbourg
CNRS
Institut Charles Sadron UPR22
Strasbourg 67000, France
E-mail: matthias.pauly@ics-cnrs.unistra.fr

Y. Battie
Université de Lorraine
LCP-A2MC, Metz 57000, France

C. Genet, T. W. Ebbesen
Université de Strasbourg
CNRS
Institut de Science et d'Ingénierie Supramoléculaires
UMR 7006
Strasbourg 67000, France

G. Decher
International Center for Materials Nanoarchitectonics
Tsukuba, Ibaraki 305-0044, Japan

G. Decher
International Center for Frontier Research in Chemistry
Strasbourg 67083, France

The ORCID identification number(s) for the author(s) of this article can be found under https://doi.org/10.1002/adom.202202831

DOI: 10.1002/adom.202202831

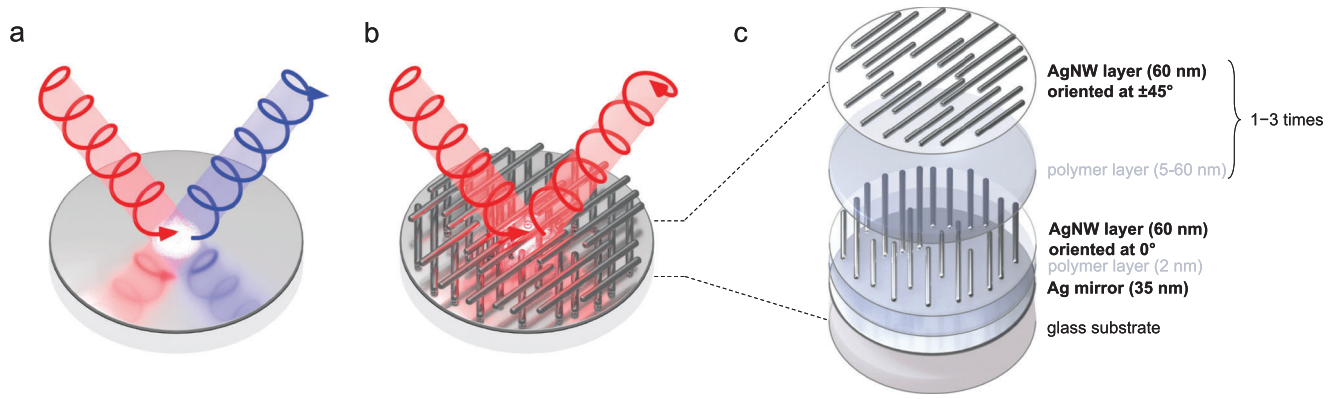

Figure 1. a) Schematic image of a conventional mirror that reverses the handedness of circularly polarized light upon reflection, b) and of a chiral mirror that preserves the handedness. c) Layer structure of a left-handed chiral mirror with the top AgNW layer oriented at +45° using grazing incidence spraying with respect to the bottom oriented AgNW layer direction. When the top AgNW layer is oriented at −45°, a right-handed mirror is obtained. A third or fourth AgNW layer separated by a polyelectrolyte multilayer spacer can be added. The thickness of the polyelectrolyte multilayer spacer between AgNW layers can be easily tuned and is varied between 5 and 60 nm.

top-down approaches. Chiral assembly of individual non-chiral building blocks by directed bottom-up assembly strategies has been proposed to tackle this challenge.[14] In this work, we propose an efficient, easy-to-use, and scalable bottom-up method to fabricate chiral mirrors that show differential reflection of LCP and RCP in a broadband range at UV–vis–NIR frequencies. We show in addition that the chiral reflective properties of the metasurfaces can be easily tuned by varying the 3D structure of the metamirrors at nano- and mesoscale level.

The chiral mirrors are fabricated by depositing twisted layers of oriented silver nanowires (AgNWs) on a conventional metallic silver mirror (Figure 1c). This is realized by using two techniques, namely Layer-by-Layer (LbL) assembly and Grazing Incidence Spraying (GIS). LbL assembly is a broadly used approach for the fabrication of stratified multimaterial films and composites,[15] while GIS involves the deposition of anisotropic 1D nano-objects by spraying a suspension of those objects on a substrate at a small incidence angle.[16] It has been proven to be effective in fabricating highly oriented films for a variety of building blocks ranging from silver nanowires,[16–17] gold nanorods (AuNRs),[18] metal oxide nanowires,[19] cellulose nanofibers,[20] and silica helices coated with gold nanoparticles.[21] We have previously reported that chiral plasmonic Bouligand nanostructures with giant circular dichroism and birefringence as well as tunable chiroptical properties can be prepared by combining LbL and GIS of AgNWs or AuNRs,[22] whose hierarchical structural arrangement and associated circular dichroism can be controlled by macroscopic tools in the fabrication process. These superstructures consist of 2 or more layers of aligned plasmonic 1D nano-objects,[23] whose orientation direction is rotated with respect to neighboring layers. Left-handed (LH) and right-handed (RH) structures are defined by the rotation handedness of the helical assembly. While dense AgNW layers are semi-reflecting, the giant chiroptical properties of those Bouligand chiral metasurfaces based on AgNWs (similarly to other twisted layers of 1D anisotropic plasmonic nanomaterials[24]) were only investigated in transmission.[22] In the present report, we focus on the structure-dependent polarized reflection of such Bouligand architectures deposited on a semi-reflective metallic mirror. The resulting samples combine the circular dichroic effects of the chiral plasmonic superstructures and the reflectiveness of the underlying substrate. These chiral metasurfaces display a strong differential reflectance for circularly polarized light in a broad wavelength range in the UV–vis–NIR domain, which can be tuned by controlling the nanostructure of the Bouligand assembly.

2. Results and Discussion

2.1. Effect of Mirror Handedness

The fabrication of the chiral mirrors relies on the deposition of two, three, or four (or even more) layers of AgNWs (diameter = 60 nm) aligned in different directions on top of a silver mirror (30 nm thick silver film on a 5 nm chromium adhesion layer) sputtered on a glass substrate, arranged in clockwise (LH) or anticlockwise (RH) rotation. Each AgNW oriented monolayer displays highly anisotropic optical properties, as the transverse localized surface plasmon resonance (LSPR) modes (350 and 380 nm) are selectively excited with light linearly polarized perpendicularly to the nanowire orientation direction.[16] When light is polarized along the nanowire axis, it is mostly reflected in the near IR due to the negative real part of the dielectric function of silver (Figure S2, Supporting Information). The relative angle between adjacent layers of AgNWs is set at ±45°, which was shown to generate the highest CD in transmission.[22b] The AgNW layers are separated by a 13 nm thin LbL-assembled polyelectrolyte multilayer film, whose thickness can be finely tuned at nanometer precision by varying the number of deposited layers of polycation (poly(allylamine hydrochloride), PAH) and polyanion (poly(sodium styrene sulfonate), PSS).

Figure 2 displays the reflectance spectra depending on the input and output polarization state for an AgNW oriented monolayer and 2-layer twisted LH and RH thin films separated by a 13 nm polyelectrolyte spacer. The spectra were measured by Mueller Matrix Polarimetry in reflection mode, from which the polarization-resolved reflectance spectra were calculated (Equations S1–S5, Supporting Information). The angle of incidence is set to 60°. Modeling was performed using a Berreman transfer

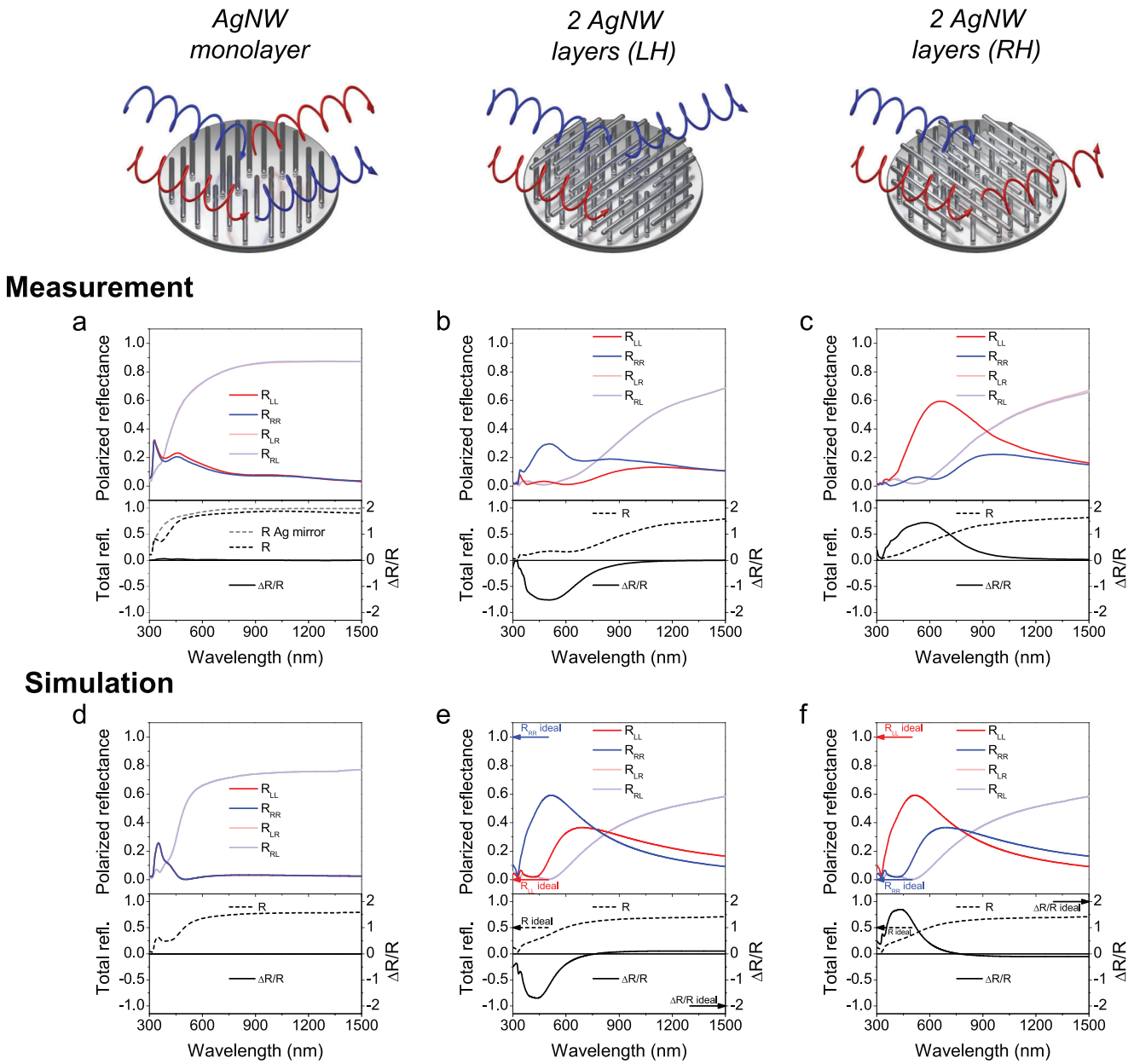

Figure 2. Measured (a–c) and modeled (d–f) reflectance spectra of an oriented monolayer of AgNWs (a,d) and of two layers of AgNWs oriented at +45° (left-handed structure (b,e) and at −45° (right-handed structure (c,f) deposited on a continuous Ag thin film. The reflection of the top panels is shown depending on i) the handedness of the incoming and o) outcoming light polarization, labeled as R_{io}, while the differential reflectance $\frac{\Delta R}{R} = \frac{R_{LCP}-R_{RCP}}{R}$ and total reflection $R = \frac{R_{LCP}+R_{RCP}}{2}$ are given in the bottom panels. The reflectance of the bare silver mirror is also given in (a). The arrows in (e) and (f) indicate the expected behavior for an ideal chiral mirror ($R_{RR} = 1$, $R_{LL} = 0$, $R = 0.5$, and $\frac{\Delta R}{R} = -2$ for the left-handed sample and $R_{LL} = 1$, $R_{RR} = 0$, $R = 0.5$, and $\frac{\Delta R}{R} = 2$ for the right-handed sample).

matrix approach[25] (see Section S2, Supporting Information) based on the measured effective complex dielectric function of an oriented AgNW monolayer (Figure S2, Supporting Information). The different spectra are labeled with the input polarization followed by the output polarization: for example, R_{RL} stands for incoming RCP light being reflected as LCP light (handedness reversed), while R_{RR} stands for incoming RCP light being reflected as RCP light (handedness preserved). The reflectance of RCP and LCP light is equal to $R_{RCP} = R_{RR} + R_{RL}$ and $R_{LCP} = R_{LL} + R_{LR}$. The total reflectance is defined as $R = \frac{R_{RCP}+R_{LCP}}{2}$ and the differential reflectance $\frac{\Delta R}{R} = \frac{R_{LCP}-R_{RCP}}{R}$. For a non-chiral sample, it is expected that $R_{RR} = R_{LL}$ and $R_{RL} = R_{LR}$, and thus $R_{RCP} = R_{LCP}$ and $\frac{\Delta R}{R} = 0$. In particular, a conventional ideal mirror totally reflects circular polarized light and reverses its polarization, thus $R_{RR} = R_{LL} = 0$ and $R_{RL} = R_{LR} = 1$. On the contrary, for a chiral sample that

selectively reflects one circular polarization without reversing it (for instance right-handed polarization), $R_{RR} = 1$, $R_{LL} = 0$ and $R_{RL} = R_{LR}$, and thus $R = 0.5$ and $\frac{\Delta R}{R} = 2$.

The reflectance of the non-chiral oriented monolayer sample deposited on a silver mirror shows both in the measured (Figure 2a) and modeled (Figure 2d) spectra a high reflectance that is independent of the incoming polarization ($R_{LL} = R_{RR}$ and $R_{LR} = R_{RL}$). As expected for a non-chiral mirror, the differential reflectance $\frac{\Delta R}{R}$ is equal to zero (Figure 2a, bottom panel). The AgNW layer only slightly reduces the total reflectance R compared to the bare silver mirror. Furthermore, the circular polarization of light is partially reversed upon reflection ($R_{LR} > R_{LL}$ and $R_{RL} > R_{RR}$) in the visible range.

On the contrary, the chiral metamirrors show polarization-dependent reflection spectra that are symmetric for LH and RH samples (Figure 2b,c, respectively). Light with a handedness opposite to that of the nanostructure is preferentially reflected, i.e., $R_{RR} > R_{LL}$ for the LH sample (Figure 2b), and $R_{LL} > R_{RR}$ for the RH sample (Figure 2c). Furthermore, the handedness of light is preserved upon reflection in the visible range ($R_{LR} = R_{RL}$, and $R_{RR} > R_{RL}$ for the LH sample and $R_{LL} > R_{LR}$ for the RH sample), while the properties in the NIR range are similar to non-chiral mirrors. This reflects in a negative peak in the differential reflectance $\frac{\Delta R}{R}$ for the LH sample and a positive peak for the RH sample, with a maximum value of $|\frac{\Delta R}{R}| \approx 1.5$ around 500 nm. Note that a mirror with maximum polarization efficiency ($R_{LL} = 1$, $R_{RR} = 0$ and $R_{RL} = R_{LR}$ for a RH sample) gives a total reflectance $R = 0.5$ and a differential reflectance $\frac{\Delta R}{R} = 2$. In other words, the polarization efficiency of such a simple 2-layer oriented AgNW structure on top of an Ag thin film reaches 75% of the maximum possible value. This highly polarized reflectance covers the entire visible range (330–1100 nm). To the best of our knowledge, this is the first report of a handedness-preserving chiral mirror whose chiral reflection covers the entire visible range. The transmittance and reflectance as well as the differential transmittance and reflectance are given up to 2000 nm in Figure S3 (Supporting Information).

Modeling is in good agreement with the experimental results; in particular, the symmetrical differential reflectance of LH and RH structures are well reproduced (Figure 2e,f). No coupling of the LSPR modes is included in the Berreman transfer matrix approach used for simulation, and the chiroptical properties can thus be well modeled by considering the AgNW monolayers as independent linear dichroic and birefringent filters stacked hierarchically one above another in a helical fashion. However, the fact that plasmonic coupling can happen between the AgNW layers and/or the Ag mirror layer may explain the difference in amplitude as well as the exact positions of peaks appearing in measurements and simulation. The slight difference in the AgNW layer thickness or density and interlayer spacing between modeling and experimental samples can also contribute to the difference between measurements and simulations. We have indeed previously demonstrated that the interlayer spacing plays a critical role in the shape of the CD spectra, similarly to what can be observed for Fabry–Perot interferences.[22b] The polarized reflectance spectra were measured and modeled with an incidence angle of 60°. The modeled angle-dependent spectra show that the polarized reflectance is almost independent of the incidence angle in the 0–60° range (Figure S4, Supporting Information). This is also confirmed by the measurement as a function of the angle of incidence in the 45–60° range (Figure S5, Supporting Information).

2.2. Effect of the Spacing between the Oriented AgNW Layers

We have demonstrated previously that the interlayer spacing between two layers of AgNWs can be finely tuned at nanometer precision by controlling the number of layers of the polyelectrolyte film between them.[22b] Here we vary the interlayer spacing d from 5 to 60 nm in a multilayer stack containing two layers of AgNWs oriented at +45° (left-handed structure), and compare the optical properties to the one described in the previous section for a LH sample with a spacing of 13 nm (**Figure 3**).

The total reflectance R of the mirror is reduced by increasing the interlayer spacing because of Fabry–Perot-type multiple reflections emerging at larger interlayer spacing, as already shown in transmission.[22b] Compared to the small change in total reflectance, the interlayer spacing has a major effect on the polarized reflectance spectra and thus on the differential reflectance. From d = 5 nm (Figure 3a) to d = 13 nm (Figure 3b), the differential reflectance peak is largely broadened, and its magnitude is doubled. For d = 60 nm (Figure 3c), the chiral reflection peak not only extends further, but also splits into a double peak. We observe a dip at 570 nm, where the differential reflection is close to 0. The peak at 860 nm has an exceptionally high value of $\Delta R/R = -1.90$, i.e., 95% of the maximum possible polarization efficiency. At this wavelength, RCP light is efficiently reflected without handedness reversal ($R_{RR} = 0.45$ and $R_{RL} < 0.01$), while the reflectance of LCP is almost zero ($R_{LL} < 0.01$ and $R_{LR} < 0.01$). The measured spectra are in good agreement with the modeled ones (Figure S6, Supporting Information).

2.3. Effect of the Number of Oriented AgNW Layers

Using LbL assembly, it is possible to prepare multilayer structures containing unlimited layers of AgNWs. In the present work, we have limited ourselves to four layers of AgNWs at maximum, since a large number of AgNW layers causes high absorption and scattering and thus reduces the total reflectance. Therefore, we varied the number of AgNW layers from 2 to 4, while keeping the interlayer spacing at 13 nm and the relative angle fixed at +45° (LH samples, **Figure 4**). For this twisting angle, a sample with four oriented AgNW layers make a Bouligand structure with a full turn of the helix. While the total reflection is reduced when increasing the layer number from 1 to 2 (Figure 2a,b), adding more layer(s) of AgNWs beyond 2 only slightly reduces the total reflectance of the mirror (Figure 4). Compared to the chiral mirror with two AgNW layers (Figure 4a), the three-layer sample has a lower differential reflectance, but it covers a larger wavelength range (Figure 4b). More interestingly, the differential reflectance of the four-layer structure changes its sign at 700 nm, being positive in the visible range and negative in the near infrared. A similar effect was also measured in transmission, with the sign of the CD spectra being reversed when more oriented AgNW layers

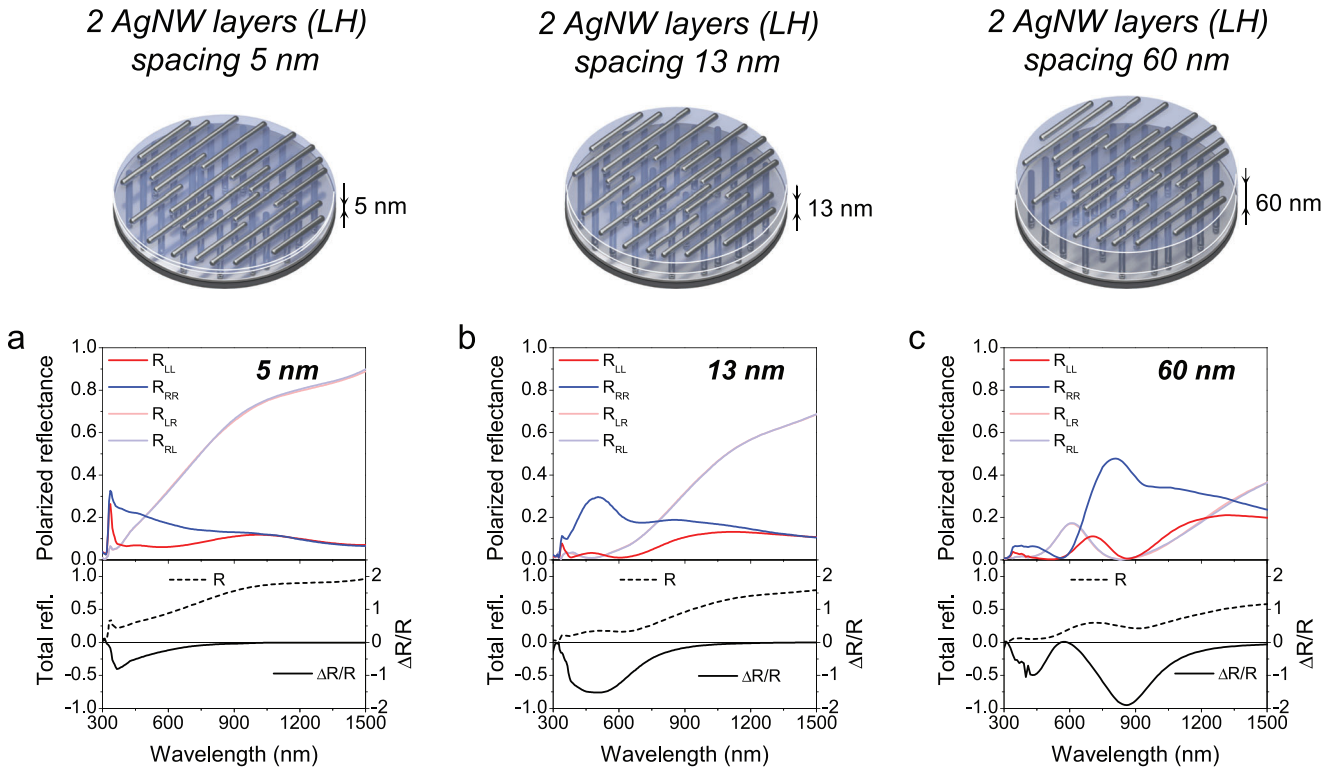

Figure 3. Spectra of the measured reflectance R labeled as function of the incoming and outgoing polarization states R_{io} and of the total reflectance R and the differential reflectance $\frac{\Delta R}{R}$ for samples consisting of two layers of AgNWs oriented at +45° (left-handed structure) deposited on top of silver mirror. The spacing between the AgNW layers is equal to a) 5 nm, b) 13 nm, and c) 60 nm. Note that the sample in (b) is the same as the one of Figure 2b.

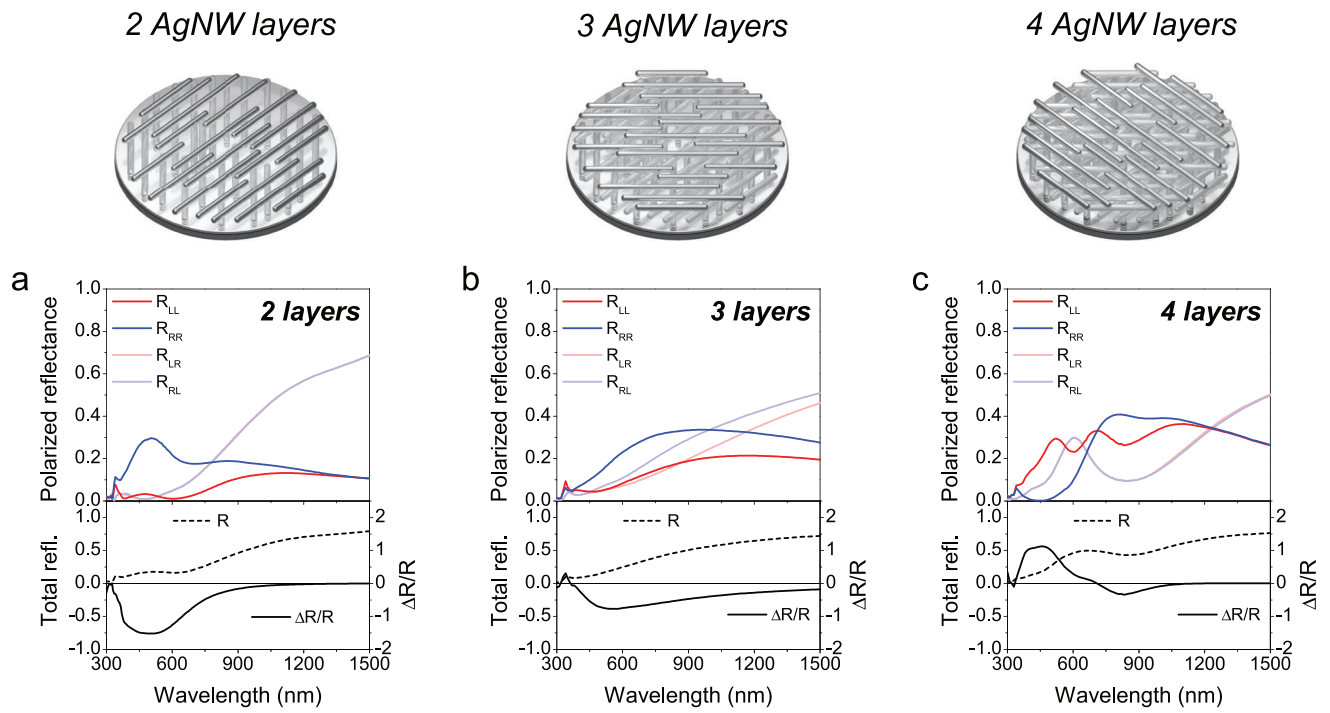

Figure 4. Spectra of the measured reflectance R labeled as function of the incoming and outgoing polarization states R_{io} and of the average reflectance R and the differential reflectance $\frac{\Delta R}{R}$ for samples consisting of a varying number of layers of oriented AgNWs deposited on top of a silver mirror. The AgNW layers are oriented at +45° (left-handed structure) and separated by a constant spacing of 13 nm. The sample consist of a) 2, b) 3, and c) 4 AgNW layers. Note that the sample in (a) is the same as the one of Figure 2b and Figure 3b.

were added.[22a] The measured spectra are in reasonable agreement with the simulated spectra, despite some differences for the four layers sample, possibly due to the slight variation between each AgNW layer thickness and density (Figure S7, Supporting Information).

It should be noted that all the measurements presented above were done at an angle of incidence of 60°. However, the chiroptical properties do not depend much on the angle of incidence (Figure S5, Supporting Information). Beside their chiral asymmetry, the presented nanostructures also have a linearly anisotropic character. Therefore, linear dichroism and birefringence may also be present. The spectrum of the conversion of the linear polarization from 0° to 90° R_{xy} is given in Figure S5e (Supporting Information) as function of the angle of incidence. While linear effects are significant in the near IR, they are negligible in the visible range. The linear anisotropy only slightly depends on the angle of incidence. Therefore, the circular polarization will be reflected as purely circular polarization in the visible range, while the circular polarization will be converted to elliptical polarization in the near infrared. Due to linear polarization effects, the chiral reflectance spectra may also vary when the sample is rotated (azimuth angle). The chiral reflectance spectra show only a small variation with the azimuth angle (Figure S8, Supporting Information). In particular, the spectra are identical for an azimuth of 0 and 180°, which is equivalent to a reversal of the angle of incidence.

Furthermore, the chiroptical properties are homogeneous in a large area, as shown by the mapping of the polarized reflectance done on an entire sample (Figure S9, Supporting Information). The differential reflectance at $\lambda = 800$ nm is very high in the entire area over that the two oriented AgNW layers overlap (8×15 mm^2), whereas it is almost zero in the regions where a single oriented AgNW layer is deposited.

The fact that i) the reflectance only slightly depends on the incidence angle and that ii) the reflectance does not depend on the handedness of light when the sample is achiral (linearly anisotropic) underlines the intrinsic character of the chirality. It cannot be excluded that in addition to intrinsic chiroptical effects from the structure, there may also be a contribution from extrinsic components, but the latter should be very small in comparison.

3. Conclusion

We have demonstrated in the present work an efficient strategy for fabricating chiral mirrors by using LbL assembly and GIS to prepare twisted Bouligand AgNW superstructures on a reflective metallic surface. The proposed approach is easy to implement with simple equipment, notwithstanding the fact that the obtained mirrors show a remarkable broadband chiral reflectance in the UV–vis–NIR range with an outstanding figure of merit (differential reflectance). All the multilayer samples shown here display a highly polarized reflectance over a broad wavelength range spanning the UV, visible, and near IR range, and that preserves the handedness of the incoming light upon reflection. The differential reflectance reaches exceptionally high values up to 95% of the maximum polarization efficiency. Our result demonstrate that the optical properties can be tuned (both in terms of total reflectance and differential reflectance, as well as regarding the shape of the spectra) by freely choosing during the fabrication the number of oriented AgNW layers and the spacing between those layers, including samples that reflect more RCP or LCP light depending on the wavelength range (Figure 4c). We have used a thin silver layer to build semi-reflective chiral mirrors, but it would also be possible to increase the total reflectance if thicker Ag films are used. It should be pointed out that these samples are prepared from aqueous suspensions/solutions of commercially available nanowires and polymers and can be prepared in a wet-chemistry lab using low-cost and simple equipment (at least compared to vacuum-based lithography processes). Such Layer-by-Layer assembled oriented nanowire layers have sufficient optical quality to enable new fabrication methods for optical elements on different surfaces.

These large-area chiral mirrors with tunable chiral reflectance in the broadband UV–vis–NIR range have numerous potential applications in optics, sensing, and chiral light-matter interactions. For example, adding another chiral mirror on top of the chiral superstructure would lead to a closed chiral cavity, which could generate tunable chiral cavity modes. This will pave the way for the research of chiral light–matter interactions in the strong coupling regime and has a huge potential for chiral catalysis and enantioselective synthesis.

4. Experimental Section

Materials: Poly(ethyleneimine) ($\overline{M_n} \approx 60\ 000$ g mol^{-1}) was purchased from BASF (Germany). Poly(sodium 4-styrenesulfonate) ($\overline{M_w} \approx 70\ 000$ g mol^{-1}) and poly(allylamine hydrochloride) ($\overline{M_w} \approx 15\ 000$ g mol^{-1}) were purchased from Sigma–Aldrich (Germany). Silver nanowires were purchased from ACS Material (USA).

Fabrication: The fabrication of the chiral mirrors relies on the deposition of twisted AgNW multilayer structures on a reflective metallic surface. First, 5 nm thick chromium layer and 30 nm thick silver layers were deposited successively on a glass slide by sputtering. Then, a layer of PEI was deposited on the silver mirror by spray-assisted LbL assembly. A solution of PEI (2.5 mg mL^{-1} in water) was sprayed on the silver mirror with an Air-boy spraying bottle for 10 s, followed by 10 s of water rinsing. Oriented AgNWs were afterward deposited on the PEI-coated silver mirror by GIS. A spraying nozzle (1/4J SS, Spraying Systems Co., USA) was connected to a liquid pump (M50, VICI Valco Instruments Co., USA) and an air flowmeter (Red-Y, Vögtlin Instruments GmbH, Switzerland). A suspension of AgNWs (0.2 mg mL^{-1} in water) was sprayed on the PEI-coated silver mirror at a small incidence angle of 10° for 200 s. The distance between the nozzle and the substrate was set to 1 cm. The fluid flow rate and the air flow rate were controlled at 1 mL min^{-1} and 30 L min^{-1} by the liquid pump and the air flowmeter, respectively. The sample was rinsed by spraying with water using an Air-boy spraying bottle for 10 s before drying with compressed air.

Then, a polyelectrolyte multilayer spacer with the following structure PEI/(PSS/PAH)$_n$/PSS/PEI was deposited on the oriented AgNW layer using the same spraying method as for the PEI layer. This study had previously shown that this allows tuning the thickness of the spacer with nanometer precision by varying n.[22b] Here, the thickness was varied from 5 nm (n = 1), 13 nm (n = 5) to 60 nm (n = 28). Another layer of AgNWs oriented in a different direction with respect to the first layer was deposited on the polyelectrolyte spacer by rotating the sample before spraying the new AgNW layer. The angle between the AgNW layers was set at 45° for left-handed structures and −45° for right-handed structures. The same process was repeated for the fabrication of three- and four-layer structures.

Characterization: The Mueller matrix of the samples was measured by a phase modulation ellipsometer (UVISEL). To measure the complete Mueller matrix, a quarter-wave plate was introduced in the polarization

state generator. The Mueller matrix was measured in reflection mode at an angle of incidence of 60° with a beam size is ≈500 µm unless otherwise specified. The total reflection (R) and differential reflection (ΔR) as well as R_{io} were deduced from the Mueller matrix spectra (see Section S1, Supporting Information, for more details).

Modeling: The simulations were carried out based on the Berreman transfer matrix formalism (see Section S2, Supporting Information, for more details). This formalism requires the knowledge of the dielectric function of each layer. This dielectric function was deduced from ellipsometric measurements in reflection performed on films deposited on silicon substrate (Figure S2, Supporting Information) for the polymeric and the oriented AgNW layers. The oriented AgNW monolayer exhibited a uniaxial anisotropy with an optical axis parallel to the AgNW long axis. The optical model consisted of a silver mirror covered with a multilayer structure detailed in Figure S1 (Supporting Information).

Supporting Information

Supporting Information is available from the Wiley Online Library or from the author.

Acknowledgements

The authors thank the electron microscopy core facility of the Institut Charles Sadron and the ellipsometry core facility of the LCP-A2MC (Université de Lorraine, http://lcp-a2mc.univ-lorraine.fr). W.W. acknowledges financial support from the China Scholarship Council. This work was part of the Interdisciplinary Thematic Institutes QMat and HiFunMat of the University of Strasbourg, CNRS, and Inserm. It was supported by the following programs: IdEx Unistra (ANR-10-IDEX-0002), SFRI STRATUS project (ANR-20-SFRI-0012), the Labex CSC project ANR-10-LABX-0026-CSC, the Labex NIE project ANR-11-LABX-0058-NIE, USIAS (ANR-10-IDEX- 0002-02), under the framework of the French Investments for the Future Program, and the ERC (project 788482 MOLUSC).

Conflict of Interest

The authors declare no conflict of interest.

Data Availability Statement

The data that support the findings of this study are available from the corresponding author upon reasonable request.

Keywords

bottom-up assembly, chirality, circular dichroism, circularly polarized light, metamaterials, silver nanowires

Received: November 27, 2022
Revised: May 5, 2023
Published online:

[1] a) E. Plum, N. I. Zheludev, *Appl. Phys. Lett.* **2015**, *106*, 221901; b) H. Hübener, U. De Giovannini, C. Schäfer, J. Andberger, M. Ruggenthaler, J. Faist, A. Rubio, *Nat. Mater.* **2021**, *20*, 438.
[2] L. Jing, Z. Wang, Y. Yang, B. Zheng, Y. Liu, H. Chen, *Appl. Phys. Lett.* **2017**, *110*, 231103.
[3] a) F. Zhang, J. Xu, A. Lakhtakia, S. M. Pursel, M. W. Horn, A. Wang, *Appl. Phys. Lett.* **2007**, *91*, 023102; b) J. Gautier, M. Li, T. W. Ebbesen, C. Genet, *ACS Photonics* **2022**, *9*, 778; c) K. Voronin, A. S. Taradin, M. V. Gorkunov, D. G. Baranov, *ACS Photonics* **2022**, *9*, 2652.
[4] a) J. Feis, D. Beutel, J. Köpfler, X. Garcia-Santiago, C. Rockstuhl, M. Wegener, I. Fernandez-Corbaton, *Phys. Rev. Lett.* **2020**, *124*, 033201; b) M. L. Solomon, A. A. E. Saleh, L. V. Poulikakos, J. M. Abendroth, L. F. Tadesse, J. A. Dionne, *Acc. Chem. Res.* **2020**, *53*, 588.
[5] P. Lodahl, S. Mahmoodian, S. Stobbe, A. Rauschenbeutel, P. Schneeweiss, J. Volz, H. Pichler, P. Zoller, *Nature* **2017**, *541*, 473.
[6] a) T. Chervy, S. Azzini, E. Lorchat, S. Wang, Y. Gorodetski, J. A. Hutchison, S. Berciaud, T. W. Ebbesen, C. Genet, *ACS Photonics* **2018**, *5*, 1281; b) A. Lininger, G. Palermo, A. Guglielmelli, G. Nicoletta, M. Goel, M. Hinczewski, G. Strangi, *Adv. Mater.* **2022**, https://onlinelibrary.wiley.com/doi/10.1002/adma.202107325.
[7] a) L. Kang, S. P. Rodrigues, M. Taghinejad, S. Lan, K.-T. Lee, Y. Liu, D. H. Werner, A. Urbas, W. Cai, *Nano Lett.* **2017**, *17*, 7102; b) Z. Li, W. Liu, H. Cheng, D.-Y. Choi, S. Chen, J. Tian, *Adv. Mater.* **2020**, *32*, 1907983.
[8] a) B. Semnani, J. Flannery, R. Al Maruf, M. Bajcsy, *Light: Sci. Appl.* **2020**, *9*, 23; b) H. Kwon, A. Faraon, *ACS Photonics* **2021**, *8*, 2980; c) I. Hodgkinson, Q. h. Wu, B. Knight, A. Lakhtakia, K. Robbie, *Appl. Opt.* **2000**, *39*, 642.
[9] a) S. Xiao, H. Mühlenbernd, G. Li, M. Kenney, F. Liu, T. Zentgraf, S. Zhang, J. Li, *Adv. Opt. Mater.* **2016**, *4*, 654; b) L. Mao, K. Liu, S. Zhang, T. Cao, *ACS Photonics* **2020**, *7*, 375.
[10] Z. Wang, H. Jia, K. Yao, W. Cai, H. Chen, Y. Liu, *ACS Photonics* **2016**, *3*, 2096.
[11] W. Mai, D. Zhu, Z. Gong, X. Lin, Y. Chen, J. Hu, D. H. Werner, *AIP Adv.* **2019**, *9*, 045305.
[12] a) H. Wang, Y. Li, L. Huang, Y. Jing, Q. Yuan, J. Wang, J. Zhang, S. Qu, *Ann. Phys.* **2021**, *533*, 2000515; b) W. Gao, C. Huang, Z. Feng, M. Li, J. Dong, *Opt. Express* **2021**, *29*, 33367.
[13] M. Liu, E. Plum, H. Li, S. Duan, S. Li, Q. Xu, X. Zhang, C. Zhang, C. Zou, B. Jin, J. Han, W. Zhang, *Adv. Opt. Mater.* **2020**, *8*, 2000247.
[14] a) W. Wu, M. Pauly, *Mater. Adv.* **2022**, *3*, 186; b) E. S. A. Goerlitzer, A. S. Puri, J. J. Moses, L. V. Poulikakos, N. Vogel, *Adv. Opt. Mater.* **2021**, *9*, 2100378; c) R. Xiong, S. Yu, M. J. Smith, J. Zhou, M. Krecker, L. Zhang, D. Nepal, T. J. Bunning, V. V. Tsukruk, *ACS Nano* **2019**, *13*, 9074.
[15] a) G. Decher, *Science* **1997**, *277*, 1232; b) K. Ariga, Y. Lvov, G. Decher, *Phys. Chem. Chem. Phys.* **2022**, *24*, 4097; c) J. J. Richardson, J. Cui, M. Björnmalm, J. A. Braunger, H. Ejima, F. Caruso, *Chem. Rev.* **2016**, *116*, 14828.
[16] H. Hu, M. Pauly, O. Felix, G. Decher, *Nanoscale* **2017**, *9*, 1307.
[17] P. T. Probst, S. Sekar, T. A. F. König, P. Formanek, G. Decher, A. Fery, M. Pauly, *ACS Appl. Mater. Interfaces* **2018**, *10*, 3046.
[18] S. Sekar, V. Lemaire, H. Hu, G. Decher, M. Pauly, *Faraday Discuss.* **2016**, *191*, 373.
[19] M. Taner Camci, M. Pauly, C. Lefevre, C. Bouillet, M. Maaloum, G. Decher, D. Martel, *Nanoscale* **2021**, *13*, 8958.
[20] R. Blell, X. Lin, T. Lindström, M. Ankerfors, M. Pauly, O. Felix, G. Decher, *ACS Nano* **2017**, *11*, 84.
[21] J. Gao, W. Wu, V. Lemaire, A. Carvalho, S. Nlate, T. Buffeteau, R. Oda, Y. Battie, M. Pauly, E. Pouget, *ACS Nano* **2020**, *14*, 4111.
[22] a) H. Hu, S. Sekar, W. Wu, Y. Battie, V. Lemaire, O. Arteaga, L. V. Poulikakos, D. J. Norris, H. Giessen, G. Decher, M. Pauly, *ACS Nano* **2021**, *15*, 13653; b) W. Wu, Y. Battie, V. Lemaire, G. Decher, M. Pauly, *Nano Lett.* **2021**, *21*, 8298.
[23] H. Hu, S. Wang, X. Feng, M. Pauly, G. Decher, Y. Long, *Chem. Soc. Rev.* **2020**, *49*, 509.
[24] a) P. T. Probst, M. Mayer, V. Gupta, A. M. Steiner, Z. Zhou, G. K. Auernhammer, T. A. F. König, A. Fery, *Nat. Mater.* **2021**, *20*, 1024; b) Y. Zhao, M. A. Belkin, A. Alù, *Nat. Commun.* **2012**, *3*, 870; c) X. Yin, M. Schäferling, B. Metzger, H. Giessen, *Nano Lett.* **2013**, *13*, 6238.
[25] M. Schubert, *Phys. Rev. B* **1996**, *53*, 4265.